

Analysis of HST/COS spectra of the bare C-O stellar core H1504+65 and a high-velocity twin in the Galactic halo[★]

K. Werner and T. Rauch

Institute for Astronomy and Astrophysics, Kepler Center for Astro and Particle Physics, Eberhard Karls Universität Tübingen, Sand 1, 72076 Tübingen, Germany
e-mail: werner@astro.uni-tuebingen.de

Received 27 August 2015 / Accepted 25 September 2015

ABSTRACT

H1504+65 is an extremely hot white dwarf (effective temperature $T_{\text{eff}} = 200\,000\text{ K}$) with a carbon-oxygen dominated atmosphere devoid of hydrogen and helium. This atmospheric composition was hitherto unique among hot white dwarfs (WDs), and it could be related to recently detected cooler WDs with C or O dominated spectra. The origin of the H and He deficiency in H1504+65 is unclear. To further assess this problem, we performed ultraviolet spectroscopy with the Cosmic Origins Spectrograph (COS) aboard the Hubble Space Telescope (HST). In accordance with previous far-ultraviolet spectroscopy performed with the Far Ultraviolet Spectroscopic Explorer, the most prominent lines stem from C IV, O V–VI, and Ne VI–VIII. Archival HST/COS spectra are utilised to prove that, considering its exotic composition, the supersoft X-ray source RX J0439.8–6809 is an even hotter ($T_{\text{eff}} = 250\,000\text{ K}$) twin of H1504+65. In contrast to earlier claims, we find that the star is not located in the Large Magellanic Cloud, but is a foreground object in the Galactic halo at a distance of 9.2 kpc, 5.6 kpc below the Galactic plane, receding with $v_{\text{rad}} = +220\text{ km s}^{-1}$.

Key words. stars: individual: H1504+65 – stars: individual: RX J0439.8–6809 – stars: abundances – stars: atmospheres – stars: evolution – stars: AGB and post-AGB – white dwarfs

1. Introduction

H1504+65 was discovered as a very bright soft X-ray source by HEAO1¹ (Nugent et al. 1983) and its blue optical counterpart was detected by Nousek et al. (1986). It was argued that the source is an extremely hot white dwarf ($T_{\text{eff}} = 160\,000 \pm 30\,000\text{ K}$ and surface gravity $\log(g/\text{cm s}^{-2}) = 7.5 \pm 0.5$) that is devoid of hydrogen and helium as a result of the lack of respective lines in the optical spectrum. Non-local thermodynamic equilibrium (non-LTE) modelling of ultraviolet (UV) and optical spectra proved the high temperature and showed that the atmosphere is mainly composed by carbon and oxygen in equal amounts (Werner 1991). Over the years, substantial efforts were made with subsequent spectroscopy in the soft X-ray range (with EUVE² and Chandra observatories), in the UV (HUT³, FUSE⁴, HST⁵), and in the optical with large ground-based telescopes (Werner & Wolff 1999; Werner et al. 2004a,b, 2007, 2010). These efforts lead to tight constraints on effective temperature and gravity ($T_{\text{eff}} = 200\,000 \pm 20\,000\text{ K}$, $\log g = 8.0 \pm 0.5$) and the detection of high amounts of neon (2–5 %, by mass) and magnesium (2 %) as well as iron at solar abundance level. High-resolution UV spectroscopy presented in this paper was performed with the aim to further constrain the trace ele-

ment abundances and to shed more light on the origin of the exotic composition of H1504+65.

Spectroscopically, H1504+65 was classified as a PG 1159 star, denoting hot ($T_{\text{eff}} = 75\,000\text{--}200\,000\text{ K}$), hydrogen-deficient (pre-)white dwarfs (WDs) that suffered a late helium-shell flash, causing He-C dominated atmospheres with high admixtures of oxygen (He = 0.30–0.85, C = 0.13–0.60, O = 0.02–0.20, Werner & Herwig 2006). H1504+65 is an extreme member of this class because of its helium-deficiency (He < 0.01, C = 0.5, O = 0.5). We argued that the extreme abundances are perhaps the consequence of additional, strong mass loss, eroding the star down to its C-O core or, alternatively, that the star is the result of a binary WD merger. It could also be that this most massive known PG 1159 star ($M = 0.84^{+0.13}_{-0.10} M_{\odot}$) emerged from a relatively massive main-sequence star (8 – 10 M_{\odot}), which evolved into a carbon-burning, super-AGB star (e.g. García-Berro et al. 1997; Doherty et al. 2015; Woosley & Heger 2015).

As to its future evolution, we speculated that H1504+65, should it have retained traces of helium in its envelope, would evolve into a pure-He atmosphere (DB) white dwarf and later into a DQ white dwarf, which exhibits traces of C due to dredge-up by a thin, convective He-envelope (Koester et al. 1982). More drastic examples of possible cooled-down versions of H1504+65 were found recently, namely, the so-called hot DQ white dwarfs ($T_{\text{eff}} = 18\,000\text{--}24\,000\text{ K}$, Dufour et al. 2007, 2011) with carbon-dominated atmospheres. In addition, helium-dominated WDs with O-rich atmospheres were discovered and they are interpreted as almost naked O-Ne stellar cores ($T_{\text{eff}} \approx 10\,000\text{ K}$, Gänsicke et al. 2010; Kepler et al. 2015).

Although the number of known PG 1159 stars has increased to about 50 in the recent years, mainly as a result of the Sloan Digital Sky Survey (Werner et al. 2014), H1504+65 re-

[★] Based on observations with the NASA/ESA Hubble Space Telescope, obtained at the Space Telescope Science Institute, which is operated by the Association of Universities for Research in Astronomy, Inc., under NASA contract NAS5-26666.

¹ High Energy Astronomy Observatory 1

² Extreme Ultraviolet Explorer

³ Hopkins Ultraviolet Telescope

⁴ Far Ultraviolet Spectroscopic Explorer

⁵ Hubble Space Telescope

Table 1. Observation log of HST/COS spectroscopy of H1504+65 and RX J0439.8–6809.^a

Star	Dataset	Grating	$\lambda/\text{\AA}$ [A]	$\lambda/\text{\AA}$ [B]	t_{exp}/s
H1504	LB3351010	G130M	1133–1279	1288–1433	1560
	LB3351020	G160M	1407–1587	1598–1777	2773
J0439	LCB501010	G130M	1133–1279	1288–1433	14080

Notes. ^(a) Columns 4 and 5 give the wavelength ranges covered by detector segments A and B. Exposure times are given in the last column.

mained a unique object. However, another soft X-ray source was suspected of being a similar object since some time ago. RX J0439.8–6809 was discovered by ROSAT and classified as a persistent supersoft X-ray source most probably located in the Large Magellanic Cloud (LMC; Greiner et al. 1994) and the blue optical counterpart was detected by van Teeseling et al. (1996). The spectral energy distribution was found to be consistent with a WD with $T_{\text{eff}} \approx 300\,000\text{ K}$. A UV spectrum taken by van Teeseling et al. (1999) with HST/STIS⁶ is rather featureless. No flux variability was detected. It was argued that the source is either a supersoft X-ray binary powered by stable nuclear shell burning or a single hot pre-white dwarf approaching the WD cooling sequence. The idea that the source might be similar to H1504+65 was corroborated with optical spectroscopy (Reinsch et al. 2002), which revealed, among others, O VI emission lines. They were found redshifted by $250 \pm 30\text{ km s}^{-1}$.

In the following, we describe the HST observations (Sect. 2) and model atmospheres (Sect. 3) utilised for the spectral analysis, which is presented in Sects. 4 and 5 for H1504+65 and RX J0439.8–6809, respectively. Stellar parameters and distances are derived in Sect. 6. We summarise the results and conclude in Sect. 7.

2. Observations

HST far-ultraviolet spectroscopy of H1504+65 with the Cosmic Origins Spectrograph (COS), using gratings G130M and G160M at central wavelength settings 1291 and 1600 Å, respectively, was performed during Cycle 17. They were conducted during two consecutive orbits on May 25, 2010. Table 1 summarises the observations. The resolving power $\lambda/\Delta\lambda$ of the G130M and G160M gratings across the observed wavelength ranges is 15 000–19 000 and 15 000–21 000, respectively, corresponding to $\Delta\lambda \approx 0.08$ and 0.09 Å , respectively. The spectra were corrected for the radial velocity of the star ($+44 \pm 4\text{ km s}^{-1}$) for comparison with our synthetic spectra. As measured from the Lyman α wings, the hydrogen column density towards H1504+65 is $N_{\text{HI}} = 6.0 \times 10^{19}\text{ cm}^{-2}$, identical with a result from previous HUT observations (Kruk & Werner 1998). The spectrum is shown in Fig. 1.

The HST/COS spectrum of RX J0439.8–6809 was retrieved from the MAST archive (Proposal ID 13289). The observation was performed on Jan. 10, 2014 with the G130M grating in the same set-up as our observation of H1504+65, with an exposure time of 14 080 s, however, only for one central wavelength setting (1291 Å). The spectrum was corrected for the radial velocity of the star ($v_{\text{rad}} = +220 \pm 10\text{ km s}^{-1}$) for comparison with synthetic spectra. This velocity is consistent with that measured from optical spectra ($+250 \pm 30\text{ km s}^{-1}$; see Introduction) and is close to the radial velocity of the LMC ($+262$

Table 2. Number of levels and lines of model ions used for line formation calculations of metals.^a

	III	IV	V	VI	VII	VIII
C	1,0	54,291				
N		16,30	54,297			
O		1,0	12,18	54,291		
Ne				92,687	103,761	77,510
Mg			15,18	27,60	46,147	50,269
Si			25,59	45,193	61,138	55,239
	VIII	IX	X	XI		
Ca	1,0	15,23	25,126	4,2		

Notes. ^(a) First and second number of each table entry denote the number of levels and lines, respectively. Not listed for each element is the highest ionisation stage, which only comprises its ground state. For the treatment of iron, see text.

km s^{-1} ; McConnachie 2012). The low-ionisation interstellar absorption lines (C II, Si II, S II, Fe II) have $v_{\text{rad}} = +8 \pm 5\text{ km s}^{-1}$. The strongest of them display a second, much weaker velocity component with $v_{\text{rad}} = +150 \pm 10\text{ km s}^{-1}$, which probably stems from a high-velocity cloud in the Galactic halo (see e.g. Richter et al. 1999; Smoker et al. 2015). These high-velocity interstellar components are not uncommon in UV spectra of very hot pre-white dwarfs, as, for instance, encountered in a recent study of four H-deficient objects with distances 2–8 kpc (Reindl et al. 2014). One of these (HS 1522+6615) is a halo object 7.9 kpc away (5.5 kpc from the Galactic plane) with a high radial velocity of -180 km s^{-1} .

The spectrum of RX J0439.8–6809 is contaminated by strong airglow lines. Besides Lyman α , there are strong emissions from N I (at 1134/1135 and 1200 Å) and O I (at 1302/1306 and 1356/1358 Å); see the airglow line table on the COS instrument page⁷. As measured from the Lyman α wings, the interstellar hydrogen column density towards RX J0439.8–6809 is $N_{\text{HI}} = 3.5 \times 10^{20}\text{ cm}^{-2}$, consistent with the previous result from a HST/STIS observation ($4 \times 10^{20}\text{ cm}^{-2}$, van Teeseling et al. 1999). The spectrum is shown in Fig. 2.

⁷ http://www.stsci.edu/hst/cos/calibration/airglow_table.html

⁶ Space Telescope Imaging Spectrograph

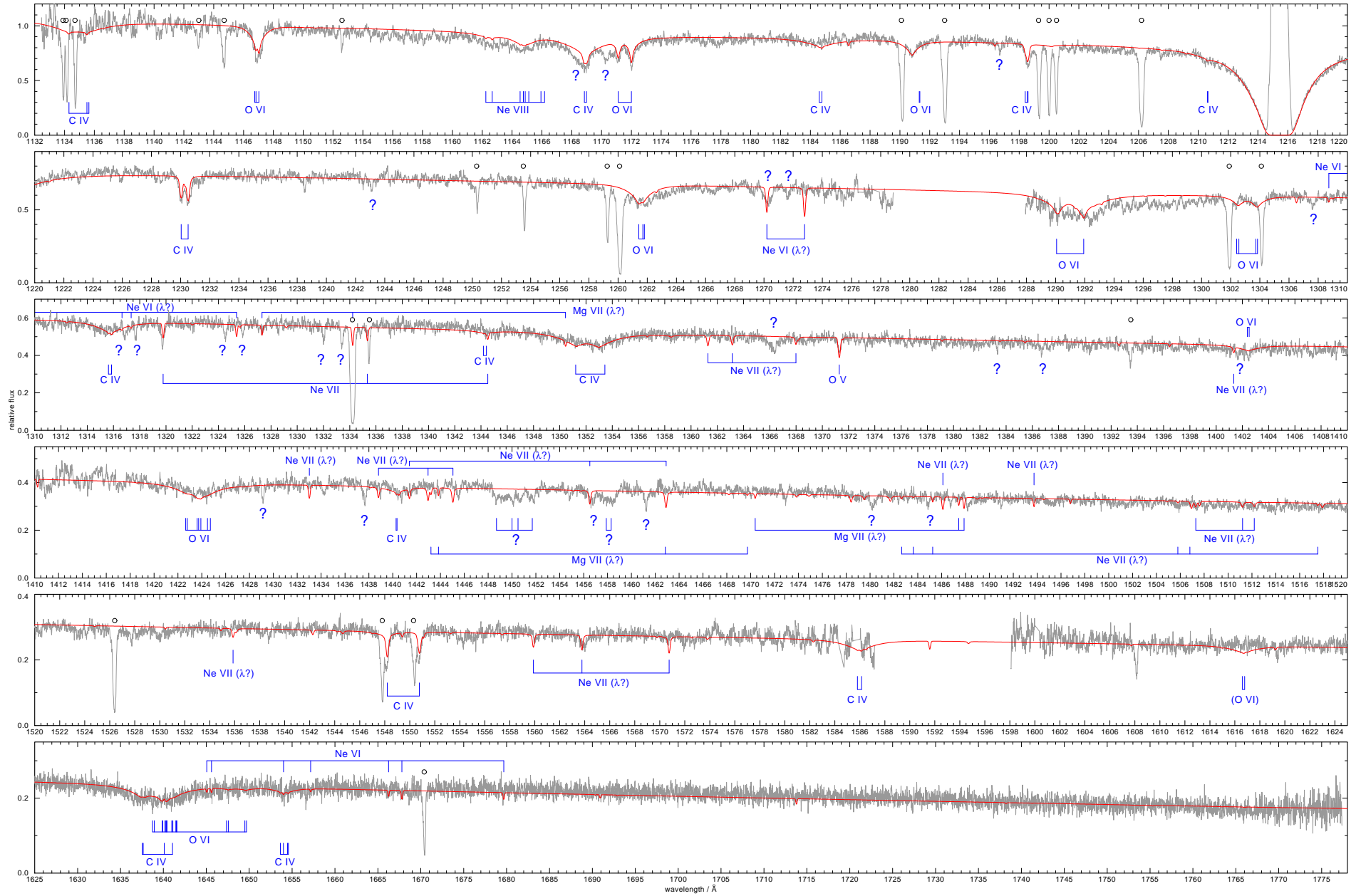


Fig. 1. HST/COS spectrum of H1504+65 and a model ($T_{\text{eff}} = 200\,000\text{ K}$, $\log g = 8$, $C = 0.46$, $O = 0.46$, $Ne = 0.06$, $Mg = 0.02$). Observation and model were folded with 0.02 \AA and 0.1 \AA Gaussians, respectively. Unidentified photospheric lines are marked with “?”. Other observed narrow lines are of interstellar origin (the strongest are marked with circles). “ $\lambda?$ ” denotes lines in the model with uncertain wavelength position.

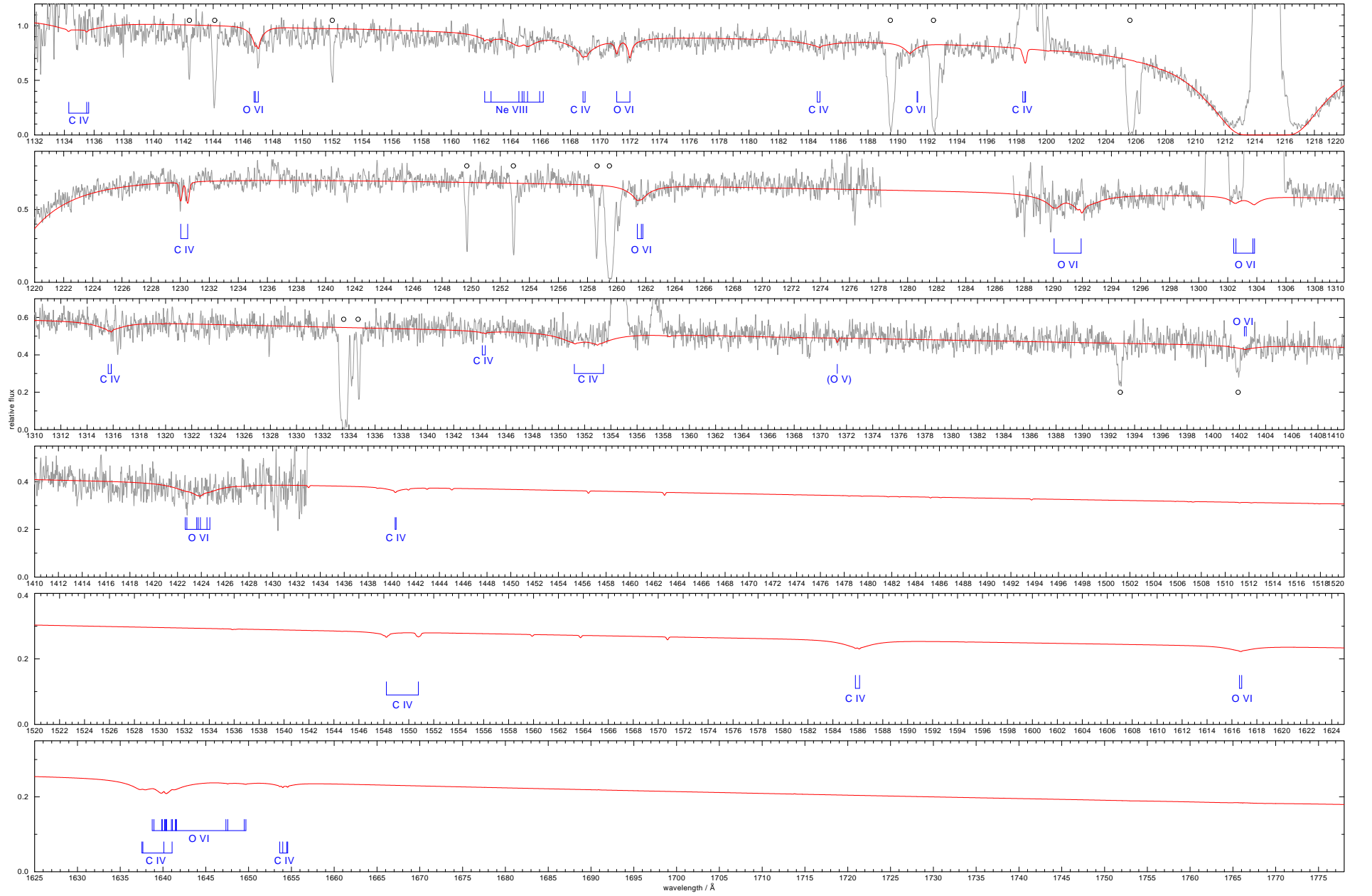


Fig. 2. HST/COS spectrum of RX J0439.8–6809 and a model ($T_{\text{eff}} = 250\,000\text{ K}$, $\log g = 8$, $C = 0.495$, $O = 0.495$, $\text{Ne} = 0.01$). Observation and model were folded with 0.05 Å and 0.1 Å Gaussians, respectively. Unidentified photospheric lines are marked with "??". Other observed narrow lines are of interstellar origin (the strongest are marked with circles).

Table 3. Identified photospheric lines in the HST/COS spectrum of H1504+65.^a

Wavelength / Å	Ion	Transition
1134.25, 1134.30	C iv	4d – 9f
1135.50	C iv	4f – 9g
1146.75, 1146.83, 1477.03	O vi	4d – 5p
1162.24, 1162.67	Ne viii	5d – 6f
1164.54, 1164.76	Ne viii	5f – 6g
1164.88	Ne viii	5g – 6h
1168.85, 1168.99	C iv	3d – 4f
1171.12, 1172.00	O vi	4p – 5s
1171.60; ^b	Ne viii	6h ² H ^o – 8i ² I
1184.59, 1184.77	C iv	4p – 8d
1190.80, 1190.84	O vi	5s – 7p
1198.55, 1198.59	C iv	3d – 4p
1210.61, 1210.65:	C iv	4s – 7p
1230.04, 1230.52	C iv	3p – 4s
1261.42, 1261.70, 1261.80	O vi	5p – 7d
1270.3; ^c	Ne vi	2s2p ² F ^o – 2s ² ² G
1290.06, 1290.18, 1290.21	O vi	5d – 7f
1291.81, 1291.84	O vi	5f – 7g
1291.90, 1291.92	O vi	5g – 7h
1292.00, 1292.02	O vi	5g – 7f
1292.64, 1292.67, 1293.04	O vi	5f – 7d
1298. ^g	O vi	6 – 11
1302.41, 1302.46, 1302.56	O vi	5d – 7p
1303.72, 1303.84	O vi	5p – 7s
1315.62, 1315.85	C iv	4p – 7d
1319.78	Ne vii	2p ¹ P ^o – 2p ² ³ P
1344.18:, 1344.42:	C iv	4p – 7s
1351.21, 1351.29	C iv	4d – 7f
1352.97	C iv	4f – 7g
1353.43:	C iv	4f – 7d
1358.42:, 1358.47:, 1358.50:	C iv	4d – 7p
1371.29	O v	2s ¹ P ^o – 2p ¹ D
1402.38:, 1402.47:, 1402.52:	O vi	6p – 10d
1422.65, 1422.79, 1422.81	O vi	6d – 10f
1423.61, 1423.65	O vi	6g – 10h
1423.90, 1423.92	O vi	6h – 10i
1440.30, 1440.38	C iv	4s – 6p
1548.20, 1550.77	C iv	2s – 2p
1560.2:, 1563.9:, 1572.0: ^c	Ne vii	5f ³ F ^o – 6g ³ G
1585.81:, 1586.11:, 1586.14: ^e	C iv	4p – 6d
1637.54, 1637.65	C iv	4d – 6f
1638.73, 1638.91, 1638.94	O vi	6d – 9f
1639.85, 1639.91	O vi	6f – 9g
1640.10	C iv	4f – 6g
1640.32, 1640.36	O vi	6h – 9i
1640.97, 1641.09, 1641.10	O vi	6f – 9g
1645.06:, 1645.59, 1654.01: ^f , 1657.16:, 1666.24, 1667.82,		
1679.67	Ne vi	3s ⁴ P ^o – 3p ⁴ P
1653.63, 1653.99	C iv	4p – 6s
1654.46, 1654.57	C iv	4d – 6p

Notes. ^(a) Colons denote uncertain detections; ^(b) blend with O vi; ^(c) see text; ^(e) at end of spectral segment; ^(f) blend with C iv; ^(g) weak, broad depression; not included in model.

3. Model atoms and model atmospheres

For the spectral analysis, we used our non-LTE code TMAP⁸ (Werner et al. 2012) to compute plane-parallel, line-blanketed atmosphere models in radiative and hydrostatic equilibrium (Werner & Dreizler 1999; Werner et al. 2003). These include the three most abundant elements in H1504+65, namely, C, O, and Ne. Five more species (N, Mg, Si, Ca, Fe) were investigated and treated one by one as trace elements, i.e. keeping the atmospheric structure fixed. In the same manner, an extended model

atom for Ne was introduced, meaning that non-LTE population numbers were also computed for highly-excited levels, which were treated in LTE during the preceding model-atmosphere computations. Table 2 summarises the number of considered non-LTE levels and radiative transitions between them. All model atoms were built from the publicly available Tübingen Model Atom Database (TMAD⁹), comprising data from different sources, namely, Bashkin & Stoner (1975), the databases of the National Institute of Standards and Technology (NIST¹⁰), the Opacity Project (OP¹¹, Seaton et al. 1994), the IRON project (Hummer et al. 1993), CHIANTI¹² (Dere et al. 1997; Landi et al. 2013), and the Kentucky Atomic Line List¹³.

For iron, we used a statistical approach employing typically seven superlevels per ion linked by superlines together with an opacity sampling method (Anderson 1989; Rauch & Deetjen 2003). Ionisation stages VII–IX augmented by a single, ground-level stage X were considered per species. We used the complete line list of Kurucz (so-called LIN lists, comprising about 2.6×10^5 lines of the considered ions; Kurucz 1991, 2009, 2011) for the computation of the non-LTE population numbers, and the so-called POS lists (these include only the subset of lines with precisely known, experimentally observed line positions) for the final spectrum synthesis.

4. Line identifications and spectral fitting for H1504+65

Generally, our new HST/COS spectrum is dominated by lines from C iv and O vi, which are well known from, e.g. the PG 1159 prototype PG 1159–035 (Jahn et al. 2007). In addition, we see lines from Ne vi–viii. A complete list of identified lines is listed in Table 3.

In the following, we present a detailed description of the spectrum and our line fitting procedure. We began our analysis with a reference model with literature values: $T_{\text{eff}} = 200\,000$ K, $\log g = 8$, and a C/O ratio of unity. It turned out that this model already matches the observation very well. In particular, the neon and oxygen ionisation balances confirm the temperature within the previous error range ($\pm 20\,000$ K). There is no necessity to revise the C/O ratio or the surface gravity.

4.1. Carbon

The depth of the C iv resonance doublet is not quite achieved by the 200 000 K model and would favour a slightly lower temperature (180 000 K). But then the low-ionisation features of oxygen (O v 1371 Å) and neon (Ne vi lines) become slightly too deep, while the Ne viii lines become too weak. The other C iv lines match well with the exception of the 1198 and 1230 Å lines, whose wings were significantly too broad. This fact highlights a general problem with the line broadening theory. Usually, the subordinate C iv (and O vi) line profiles are well described by an approximate treatment for linear Stark broadening because they are one-electron systems. This approximation is good for lines involving levels with high principal and angular quantum numbers (n and l) because the levels are nearly degenerate. For low- l and low- n levels this treatment becomes questionable. The 1198 and 1230 Å lines are such cases; they are the 3d–4p and 3p–4s

⁹ <http://astro.uni-tuebingen.de/~TMAD>

¹⁰ <http://www.nist.gov/pml/data/asd.cfm>

¹¹ <http://cdsweb.u-strasbg.fr/topbase/topbase.html>

¹² <http://www.chiantidatabase.org>

¹³ <http://www.pa.uky.edu/~peter/atomic>

⁸ <http://astro.uni-tuebingen.de/~TMAP>

transitions, respectively. On the other hand, the 3d–4f transition at 1169 Å, involving the high-*l* 4f level, is matched very well by the model. We note that the depression in its blue wing is probably due to an unidentified line. We now treat the 1198 and 1230 Å lines with quadratic Stark effect and indeed, they fit the observations much better.

4.2. Nitrogen

From the lack of the N v 1239/1243 Å resonance doublet we can infer an upper limit of $N < 3.0 \times 10^{-5}$, which is much tighter than the previous limit derived from the absence of optical N v emission lines ($< 5.0 \times 10^{-3}$, Werner 1991).

4.3. Oxygen

The detection of the O v 1371 Å line is important because it is very temperature sensitive. Its profile is best matched by a $T_{\text{eff}} = 200\,000$ K model, while a model with 180 000 K has a profile that is definitely too deep and the line has vanished in a 220 000 K model.

We found that the Ritz wavelengths of the O vi 5s–7p doublet (1191.34 and 1191.30 Å) must be reduced by 0.5 Å to match the observed wavelengths, indicative of inaccuracies in the level energies in the atomic databases utilised. Similar corrections for a number of other UV O vi lines were made by Jahn et al. (2007) using the spectra of several PG 1159 stars (see their Tab. 6).

4.4. Neon

Neon lines of three ionisation stages (Ne vi–viii) can be identified. Our models predict a very strong Ne vi line at 1223.3 Å from the transition $5d\ ^2D - 7f\ ^2F^o$, which is not present in the observation. The line was computed with an *f*-value from OP and NIST level energies. The upper level, however, is marked as “may not be real”, so in fact the transition might not exist at all. Consequently, we omitted it from our synthetic spectra.

The next strongest Ne vi lines in our models are the $2s2p3d\ ^2F^o - 2s^25g\ ^2G$ doublet at 1272 Å. According to Kramida et al. (1999), they are located at a single observed wavelength (1271.8 ± 1.5 Å) but two (computed) Ritz wavelengths ($1270.2/1272.8 \pm 0.5$ Å) and both components have the same strength. The H1504+65 spectrum has one strong line at 1270.3 Å plus two nearby, weaker lines with similar strength at 1269.3 and 1271.6 Å. The weaker lines might be assigned to the modelled doublet because their spacing of 2.3 Å is similar to that of the Ritz wavelengths (2.6 Å), although the absolute differences (0.9 and 1.2 Å) are about twice the quoted uncertainty of 0.5 Å. Another possibility is that the doublet spacing computed by Kramida et al. (1999) is overestimated and indeed unresolvable in the H1504+65 spectrum. The strong feature at 1270.3 Å coincides with the (unresolved) laboratory measurement of Kramida et al. (1999) at 1271.8 Å within its 1.5 Å uncertainty. This is also favoured by the fact that the total equivalent width of the computed doublet better fits to the strong observed feature than to the weaker observed lines. Another Ne vi multiplet at 1645–1680 Å is much weaker but the wavelengths of the components are well known, (± 0.03 Å, Kramida et al. 1999) and the strongest components are detectable in the observation.

As to Ne vii, our models predict many lines, however, because of uncertain level energies their positions are not known

sufficiently well to be assigned to any of the unidentified observed lines. The only line of this ion with accurately known wavelength is an intercombination line at 1319.71 Å, and this line can be identified in the observed spectrum. A triplet in our synthetic spectrum at 1560–1571 Å might be assigned to nearby absorption lines in the observation with differences of about 1 Å.

The broad absorption trough at 1162–1166 Å stems from numerous Ne viii lines (Werner et al. 2007). The presence of lines from three ionisation stages of neon offers a particularly strong constraint on T_{eff} . We confirm our earlier result of $T_{\text{eff}} = 200\,000 \pm 20\,000$ K. The neon abundance is best matched with a model with $\text{Ne} = 0.06$, which is consistent with, though higher than, earlier results.

4.5. Silicon

At $T_{\text{eff}} = 200\,000$ K, silicon lines with accurately known wavelengths from ionisation stages Si v–vi are predicted by the models. Among the strongest are, for example, Si v 1251.39 and Si vi 1229.01 Å. None of these are identified in the observation. In addition, Si vii lines are also predicted (e.g. at 1236 Å), however, their wavelengths are uncertain by up to 1 Å. Nevertheless, no possible counterparts are detectable in the observation. We derive an upper abundance limit of $\text{Si} < 2.6 \times 10^{-3}$, which is four times the solar value. An unidentified line at 1148.6 Å is well matched by a Si vi $^4P - ^4D^o$ line in the model with this abundance, however, this is perhaps by a chance coincidence because the wavelength is known only within ± 0.12 Å and another line of this multiplet at 1152.8 Å is not unambiguously detected.

4.6. Magnesium

We searched for Mg lines without success. According to our models, Mg vii has the strongest lines, however, wavelength positions are not known better than about 1–2 Å. At the abundance $\text{Mg} = 0.02$ derived from the Chandra soft-X-ray spectrum (Werner et al. 2004b), UV lines of significant strength (up to 15% central depression) are predicted, most prominently the components of a $^3P^o - ^3P$ triplet at 1291–1350 Å. Hence, some of the unidentified lines could stem from this ion.

4.7. Calcium

The strongest line predicted by our models is Ca x 1159.2 Å, a component of the 4p–4d doublet. We looked for this line in the FUSE spectrum of H1504+65, consistent with an upper abundance limit of solar ($\text{Ca} < 6.4 \times 10^{-5}$, Werner et al. 2008), to no avail. The same holds for the COS spectrum where the line is not detectable either. We had tentatively detected the 4s–4p lines at 1461.2 and 1503.6 Å in the hot PG 1159 central star of NGC 246. In the COS spectrum of H1504+65 there are lines at these positions, but it is unlikely that they stem from Ca x. At solar Ca abundance, our 200 000 K model provides lines that are too weak. Even a match of the weaker component at 1503.6 Å would require Ca ten times solar, clearly at odds with the non-detection of the 1159.2 Å line. Consequently, we confirm the upper limit of solar.

4.8. Iron

A solar iron abundance was derived from Fe x lines in FUSE data (Werner et al. 2010). Our models do not predict detectable

Table 4. Unidentified photospheric lines in the HST/COS spectrum of H1504+65 and possible identifications.

Wavelength / Å	Possible id.	Remark
1148.6	Si vi	
1159.3	Ca x	
1168.5	broad dip in C iv wing	strong
1170.3		
1196.7		
1207.5		
1223.0	Si vii	
1225.2		
1225.9		
1228.3	Si vii	
1228.7	Si vii	
1243.1	Si vii	
1246.4		
1270.3	Ne vi	strong
1271.6	Ne vi	
1307.6		a
1316.9	Ne vi	
1317.7	Ne vi	
1324.5		strong
1325.8		strong
1332.0	Na vii	strong
1333.4		strong
1334.8		
1366.4	Si vii	strong ^b
1383.4		
1386.7		
1401.6	Ne vii	
1416.3	Ne vii	
1429.0		strong ^c
1434.3	Ne vii	
1435.8		
1437.6		strong
1439.0	Ne vii	
1443.6	Ne vii	
1444.0		
1445.5	Ne vii	
1449–1452		strong broad dip, many lines
1454.8		
1456–1459		strong broad dip, many lines
1461.2		strong ^c
1472.9	Ne vii	
1475.3	Mg vii	
1480.20		strong ^b
1484.9	Ne vii	
1486.75	Ne vii	
1488.2	Mg vii, Ne vii	
1491.0	Ne vi	c
1495.3	Ne vii	
1503.6	Ca x	
1538.7	Ne vi	
1543.6	Ne vi	
1554.5		broad dip
1619.4	Ne vii	

Notes. ^(a) Also present in PG 1159–035 and hot H-rich central stars; ^(b) also present in hot PG 1159 stars; ^(c) also present in the hot PG 1159 central star of NGC 246.

lines in the COS spectral range. In particular, an unidentified feature at 1619.4 Å is not a Fe vii line in the Kurucz list located at 1619.35 Å. Estimated errors for the abundances are $\pm 20\%$ for C and O and a factor of 3 for the other elements (see also Werner et al. 2004a).

4.9. Unidentified lines

A number of photospheric lines remains unidentified. The strongest of them are listed in Table 4 along with possible identifications.

5. Spectral fitting for RX J0439.8–6809

For the model fits, the spectra of H1504+65 were smoothed with 0.02 Å (FWHM) Gaussians to increase the signal-to-noise ratio (S/N). It is then about 30 but deteriorates for $\lambda > 1500$ Å. In comparison to H1504+65, the UV flux of RX J0439.8–6809 is significantly lower (about a factor of 150), but the exposure time of the G130M spectrum was nine times higher, so the S/N is about four times lower. To compensate for this, the spectrum was smoothed with a 0.05 Å Gaussian. The spectra of both stars look rather similar but as a result of the lower S/N, fewer details can be seen in RX J0439.8–6809.

5.1. Helium

The lack of helium lines in the optical spectrum of RX J0439.8–6809 was claimed as evidence for helium-deficiency. In fact, this conclusion is difficult to draw. It has been shown that the most direct signature would be the lack of a NLTE central emission reversal from He ii 4686 Å (Werner 1991). All other He ii lines are in absorption and are blended by C iv and O vi lines at virtually equal wavelengths because all of these ions are one-electron systems. The same holds for He ii 1640 Å. In order to derive a strict upper limit for the He abundance, a much better optical spectrum would be needed.

5.2. Carbon and oxygen; effective temperature

Lines from C iv and O vi are identified and their relative strengths are similar to those in H1504+65, such that we conclude C/O = 1. However, there is a significant difference. The O v 1371 Å line is lacking, indicating a higher temperature compared to H1504+65. A model with $T_{\text{eff}} = 220\,000$ K (at $\log g = 8$) is sufficiently hot to make the line so weak that it is not detectable in the observation. On the other hand, an upper limit to T_{eff} can be derived by the fact that the C iv and O vi lines become weaker with increasing temperature. We have computed models with 250 000 K and 300 000 K. The hottest model is excluded because the lines are too weak. We finally adopt $T_{\text{eff}} = 250\,000 \pm 30\,000$ K.

In the models with $T_{\text{eff}} = 200\,000$, the C iv 1548/1551 Å resonance doublet is comparable in strength with the higher excited subordinate lines, as it is observed in H1504+65. At higher temperatures, the resonance doublet becomes even weaker than the subordinate lines and it turns into emission at $T_{\text{eff}} > 250\,000$ K. This explains the non-detection of this line in the HST/STIS spectrum taken by van Teeseling et al. (1999), albeit one has to stress that the S/N ratio of that spectrum is very poor anyhow.

5.3. Nitrogen

The N v 1239/1243 Å resonance doublet is not detectable. This is in stark contrast to the detection of two N v emission lines in the optical spectrum claimed by Reinsch et al. (2002, their Fig. 1). Indeed, one of these features near 4340 Å is a Ne vii line that is usually visible in the hottest ($T_{\text{eff}} > 150\,000$ K) PG 1159 stars (Werner et al. 2007) and predicted by our $T_{\text{eff}} = 250\,000$ model for RX J0439.8–6809. For the other feature at 4945 Å,

Table 5. Results of spectral analyses of H1504+65 and RX J0439.8–6809.^a

	H1504+65	RX J0439.8	Reference ^b
$T_{\text{eff}} / \text{kK}$	200 ± 20	250 ± 30	(1), this paper
$\log g / \text{cm s}^{-2}$	8.0 ± 0.5	8.0 ± 0.5	(2)
M/M_{\odot}	$0.83^{+0.19}_{-0.15}$	$0.86^{+0.16}_{-0.13}$	this paper
d / kpc	$0.67^{+0.29}_{-0.52}$	$9.2^{+4.1}_{-7.2}$	this paper
$ z / \text{kpc}$	$0.48^{+0.21}_{-0.38}$	$5.6^{+2.5}_{-4.3}$	this paper
He	< 0.01		(1)
C	0.46	0.50	(2), this paper
N	$< 3.0 \times 10^{-5}$	$< 1.0 \times 10^{-3}$	this paper
O	0.46	0.50	(2), this paper
Ne	0.06	0.01	(3,4,5), this paper
Na	< 0.1		(4)
Mg	0.02		(4)
Al	< 0.1		(4)
Si	$< 2.6 \times 10^{-3}$		this paper
Ca	$< 6.4 \times 10^{-5}$		(6), this paper
Fe	0.0013		(7)

Notes. ^(a) Abundances in mass fractions. Stellar mass M and distance d were derived from comparison with evolutionary tracks. The parameter z is the distance from the Galactic disk. ^(b) The last column gives references to results for H1504+65; results for RX J0439.8–6809 from this paper. (1) Werner et al. (2004b); (2) Werner (1991); (3) Werner & Wolff (1999); (4) Werner et al. (2004b); (5) Werner et al. (2007); (6) Werner et al. (2008); (7) Werner et al. (2010).

however, we cannot offer an alternative identification. From the absence of the N v UV resonance doublet, we determine an upper abundance limit of $N < 0.001$ for all models in the range $T_{\text{eff}} = 200\,000\text{--}300\,000\text{ K}$. We found that models with such a low abundance do not exhibit detectable optical N v emission lines.

5.4. Neon

The wide Ne VIII absorption trough in H1504+65 is just barely visible in RX J0439.8–6809, immediately pointing at a lower neon abundance. This is not a temperature effect because the Ne VIII lines become stronger with increasing T_{eff} . The neon abundance we deduce is $\text{Ne} = 0.01$, with an estimated uncertainty of a factor of three.

6. Stellar parameters and distances

Table 5 summarises the results of our spectroscopic analysis with results from previous work. The location of both stars in the g – T_{eff} diagram is shown in Fig. 3. Also shown are evolutionary tracks for hydrogen-deficient (pre-)white dwarfs computed by Althaus et al. (2009b) from which we derive the stellar masses. The upper limits of the error ranges required extrapolation from the two most massive tracks. We find mass ranges of $0.68\text{--}1.02 M_{\odot}$ and $0.73\text{--}1.02 M_{\odot}$ for H1504+65 and RX J0439.8–6809, respectively. The marginal difference between the mass value of H1504+65 derived here and in previous work mentioned in the Introduction (Werner et al. 2004a) arises from improved evolutionary tracks.

It should be noted that the masses could suffer from systematic errors. The used evolutionary tracks represent hydrogen-deficient, He-shell burning post-AGB stars and their hot WD descendants, whereas our stars in the present study are He-

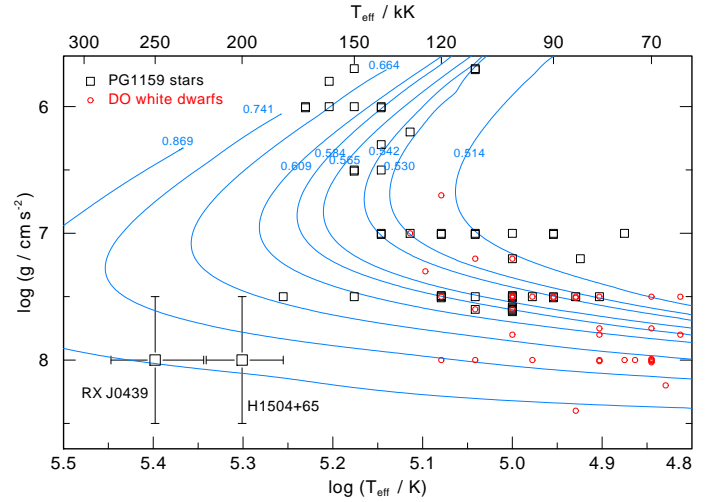


Fig. 3. Positions of H1504+65 and RX J0439.8–6809 in the g – T_{eff} diagram. Also shown are the locations of PG 1159 stars (squares) and DO white dwarfs (circles). The apparent clustering of stars at $\Delta \log g = 0.5$ steps is the consequence of employed model grids and analysis techniques that have typical errors of 0.5 dex (see, e.g. Werner & Herwig 2006). Evolutionary tracks by Althaus et al. (2009b) are labelled with the stellar mass in solar units.

Table 6. Quantities used for distance determinations.

Star	$E(B - V)$	V	V_0	H_v^e
H1504+65	0.00 ^a	16.24 ^c	16.24	3.42×10^{-3}
RX J0439.8–6809	0.09 ^b	21.74 ^d	21.65	4.30×10^{-3}

Notes. ^(a) Kruk & Werner (1998); ^(b) derived from N_{HI} , see text; ^(c) Nousek et al. (1986); ^(d) van Teeseling et al. (1996); ^(e) Eddington flux in $\text{erg cm}^{-2} \text{s}^{-1} \text{cm}^{-1}$.

deficient. Whatever the origin of the stars, the appropriate tracks would probably be different, although it may be hoped that the differences are small at the advanced, WD evolutionary state.

From $g \sim M/R^2$ and $L \sim R^2 T_{\text{eff}}^4$, we can determine the stellar radius R and luminosity L . We find that the radius of both stars is $R \approx 0.015 \pm 0.01 R_{\odot}$. They are beyond the maximum T_{eff} of their pre-WD evolution and their luminosity has dropped from about $\log(L/L_{\odot}) = 4.5$ on the horizontal part of the post-AGB evolutionary track in the HRD ($M = 0.869 M_{\odot}$ track of Althaus et al. 2009b) to $\log(L/L_{\odot}) = 2.5$ and 2.9 (H1504+65 and RX J0439.8–6809, respectively).

Distances d are computed by comparing the observed visual magnitudes with model fluxes (e.g. Heber et al. 1984), as follows:

$$d(\text{kpc}) = 7.1 \times \sqrt{H_v \cdot M \cdot 10^{0.4V_0 - \log g}},$$

where H_v is the model Eddington flux at 5400 \AA , M is the stellar mass in solar units, and V_0 is the dereddened V magnitude, $V_0 = V - 3.2 \times E(B - V)$. Reddening for RX J0439.8–6809 is computed from the relation $\log(N_{\text{HI}}/E(B - V)) = 21.58$ (Groenewegen & Lamers 1989), leading to $E(B - V) = 0.09$, in reasonable agreement with the value 0.06 derived from dust emission maps¹⁴ (Schlegel et al. 1998). The relevant quantities for the distance determination are listed in Table 6, and stellar masses, surface gravities, and the resulting distances are listed in Table 5.

¹⁴ <http://irsa.ipac.caltech.edu/applications/DUST/>

The spectroscopic distance of RX J0439.8–6809 ($9.2^{+4.1}_{-7.2}$ kpc) clearly indicates that the star is a Galactic halo object and not located in the LMC (50 kpc, Pietrzyński et al. 2013) as suspected from its location, which is roughly 1 degree off the rim of gaseous optical emission of the LMC (Greiner et al. 1994). Obviously, the direction is a chance coincidence, just like the radial velocity of the star ($+220 \pm 10 \text{ km s}^{-1}$), which is close to that of the LMC ($+262 \text{ km s}^{-1}$, McConnachie 2012). As mentioned in Sect. 2, the interstellar lines in the RX J0439.8–6809 COS spectrum have a weak, high-velocity component ($+150 \pm 10 \text{ km s}^{-1}$), which can be attributed to a Galactic high-velocity cloud. There is no component at the LMC systemic velocity.

7. Summary and conclusions

H1504+65 and RX J0439.8–6809 are the hottest known white dwarfs and they have carbon and oxygen dominated atmospheres. Their extreme surface composition is unique and the origin of this phenomenon remains mysterious. It may be significant that their masses are considerably above the WD average ($0.696 \pm 0.010 M_{\odot}$ for helium-atmosphere; i.e. DB white dwarfs, Kepler et al. 2015). Our analyses yields a maximum mass of $1.02 M_{\odot}$ for both stars, which is rather close to the minimum mass for ONeMg white dwarfs that descended from carbon-burning super-AGB stars ($1.06 M_{\odot}$; Doherty et al. 2015). Hence, they could be single high-mass white dwarfs, which for an unknown reason were eroded down to their C/O envelope. Likewise, both stars could be usual CO white dwarfs that underwent a late He-shell flash consuming the H-rich envelope and, again for an unknown reason (e.g. extreme mass loss; Schönberner & Blöcker 1992; Althaus et al. 2009a), stripped their He-envelope to expose their CO core. In both scenarios, the mass of the main-sequence progenitor is relatively large, which is difficult to reconcile with the position of RX J0439.8–6809 in the halo, unless it was ejected from the disk (e.g. by the SN explosion of a binary companion). Alternatively, the masses of H1504+65 and RX J0439.8–6809 are high enough that they could be the result of the coalescence of two CO white dwarfs (with minimum masses of $\approx 0.5 M_{\odot}$) whose H- and He-deficiency results from the merging process.

While H1504+65 is a relatively nearby WD ($d = 0.67$ kpc), RX J0439.8–6809 belongs to the Galactic halo ($|z| = 5.6$ kpc). Its distance is 9.2 kpc and, thus, it is not a member of the LMC as previously assumed. The lack of ISM lines with LMC systemic velocity corroborates this result. Its persistent soft X-ray luminosity as well as its optical non-variability (van Teeseling et al. 1999) are consistent with its nature as a single, hot white dwarf that has no active nuclear burning and is on the hot end of its WD cooling track. Consequently, its cooling rate, according to the $0.869 M_{\odot}$ post-AGB evolutionary track of Althaus et al. (2009b), is rather slow ($dT_{\text{eff}}/dt = 38 \text{ K yr}^{-1}$), and therefore, a 1% change in the UV/optical flux level takes 66 years, preventing a contemporary detection. This also explains the constant X-ray flux measured by ROSAT over three years instead of a steadily increasing X-ray flux. That was regarded as a challenge to stellar evolution theory (van Teeseling et al. 1999), however, it was based on the erroneous assumption that the star is still a very luminous, fast evolving pre-WD before entering the WD cooling sequence.

Acknowledgements. T. Rauch was supported by the German Aerospace Center (DLR) under grant 05 OR 1402. This research has made use of the SIMBAD database, operated at CDS, Strasbourg, France, and of NASA's Astrophysics

Data System Bibliographic Services. Some of the data presented in this paper were obtained from the Mikulski Archive for Space Telescopes (MAST).

References

- Althaus, L. G., Córscico, A. H., Torres, S., & García-Berro, E. 2009a, *A&A*, 494, 1021
- Althaus, L. G., Panei, J. A., Miller Bertolami, M. M., et al. 2009b, *ApJ*, 704, 1605
- Anderson, L. S. 1989, *ApJ*, 339, 558
- Bashkin, S. & Stoner, J. O. 1975, Atomic energy levels and Grotrian Diagrams - Vol.1: Hydrogen I - Phosphorus XV; Vol.2: Sulfur I - Titanium XXII
- Dere, K. P., Landi, E., Mason, H. E., Monsignori Fossi, B. C., & Young, P. R. 1997, *A&AS*, 125, 149
- Doherty, C. L., Gil-Pons, P., Siess, L., Lattanzio, J. C., & Lau, H. H. B. 2015, *MNRAS*, 446, 2599
- Dufour, P., Béland, S., Fontaine, G., Chayer, P., & Bergeron, P. 2011, *ApJ*, 733, L19
- Dufour, P., Liebert, J., Fontaine, G., & Behara, N. 2007, *Nature*, 450, 522
- Gänsicke, B. T., Koester, D., Girven, J., Marsh, T. R., & Steeghs, D. 2010, *Science*, 327, 188
- García-Berro, E., Ritossa, C., & Iben, Jr., I. 1997, *ApJ*, 485, 765
- Greiner, J., Hasinger, G., & Thomas, H.-C. 1994, *A&A*, 281, L61
- Groenewegen, M. A. T. & Lamers, H. J. G. L. M. 1989, *A&AS*, 79, 359
- Heber, U., Hunger, K., Jonas, G., & Kudritzki, R. P. 1984, *A&A*, 130, 119
- Hummer, D. G., Berrington, K. A., Eissner, W., et al. 1993, *A&A*, 279, 298
- Jahn, D., Rauch, T., Reiff, E., et al. 2007, *A&A*, 462, 281
- Kepler, S. O., Pelisoli, I., Koester, D., et al. 2015, *MNRAS*, 446, 4078
- Koester, D., Weidemann, V., & Zeidler, E.-M. 1982, *A&A*, 116, 147
- Kramida, A. E., Bastin, T., Biémont, E., Dumont, P.-D., & Garnir, H.-P. 1999, *Journal of the Optical Society of America B Optical Physics*, 16, 1966
- Kruk, J. W. & Werner, K. 1998, *ApJ*, 502, 858
- Kurucz, R. L. 1991, in *NATO ASIC Proc. 341: Stellar Atmospheres - Beyond Classical Models*, ed. L. Crivellari, I. Hubeny, & D. G. Hummer, 441
- Kurucz, R. L. 2009, in *American Institute of Physics Conference Series*, Vol. 1171, American Institute of Physics Conference Series, ed. I. Hubeny, J. M. Stone, K. MacGregor, & K. Werner, 43
- Kurucz, R. L. 2011, *Canadian Journal of Physics*, 89, 417
- Landi, E., Young, P. R., Dere, K. P., Del Zanna, G., & Mason, H. E. 2013, *ApJ*, 763, 86
- McConnachie, A. W. 2012, *AJ*, 144, 4
- Nousek, J. A., Shipman, H. L., Holberg, J. B., et al. 1986, *ApJ*, 309, 230
- Nugent, J. J., Jensen, K. A., Nousek, J. A., et al. 1983, *ApJS*, 51, 1
- Pietrzyński, G., Graczyk, D., Gieren, W., et al. 2013, *Nature*, 495, 76
- Rauch, T. & Deetjen, J. L. 2003, in *Astronomical Society of the Pacific Conference Series*, Vol. 288, *Stellar Atmosphere Modeling*, ed. I. Hubeny, D. Mihalas, & K. Werner, 103
- Reindl, N., Rauch, T., Werner, K., Kruk, J. W., & Todt, H. 2014, *A&A*, 566, A116
- Reinsch, K., Beuermann, K., & Gänsicke, B. T. 2002, in *Astronomical Society of the Pacific Conference Series*, Vol. 261, *The Physics of Cataclysmic Variables and Related Objects*, ed. B. T. Gänsicke, K. Beuermann, & K. Reinsch, 653
- Richter, P., de Boer, K. S., Widmann, H., et al. 1999, *Nature*, 402, 386
- Schlegel, D. J., Finkbeiner, D. P., & Davis, M. 1998, *ApJ*, 500, 525
- Schönberner, D. & Blöcker, T. 1992, in *Lecture Notes in Physics*, Berlin Springer Verlag, Vol. 401, *The Atmospheres of Early-Type Stars*, ed. U. Heber & C. S. Jeffery, 305
- Seaton, M. J., Yan, Y., Mihalas, D., & Pradhan, A. K. 1994, *MNRAS*, 266, 805
- Smoker, J. V., Fox, A. J., & Keenan, F. P. 2015, *MNRAS*, 451, 4346
- van Teeseling, A., Gänsicke, B. T., Beuermann, K., et al. 1999, *A&A*, 351, L27
- van Teeseling, A., Reinsch, K., & Beuermann, K. 1996, *A&A*, 307, L49
- Werner, K. 1991, *A&A*, 251, 147
- Werner, K., Deetjen, J. L., Dreizler, S., et al. 2003, in *Astronomical Society of the Pacific Conference Series*, Vol. 288, *Stellar Atmosphere Modeling*, ed. I. Hubeny, D. Mihalas, & K. Werner, 31
- Werner, K., Dreizler, S. 1999, *Journal of Computational and Applied Mathematics*, 109, 65
- Werner, K., Dreizler, S., & Rauch, T. 2012, *TMAP: Tübingen NLTE Model-Atmosphere Package*, Astrophysics Source Code Library
- Werner, K. & Herwig, F. 2006, *PASP*, 118, 183
- Werner, K., Rauch, T., Barstow, M. A., & Kruk, J. W. 2004a, *A&A*, 421, 1169
- Werner, K., Rauch, T., & Kepler, S. O. 2014, *A&A*, 564, A53
- Werner, K., Rauch, T., & Kruk, J. W. 2007, *A&A*, 474, 591
- Werner, K., Rauch, T., & Kruk, J. W. 2008, *A&A*, 492, L43
- Werner, K., Rauch, T., & Kruk, J. W. 2010, *ApJ*, 719, L32
- Werner, K., Rauch, T., Reiff, E., Kruk, J. W., & Napiwotzki, R. 2004b, *A&A*, 427, 685
- Werner, K. & Wolff, B. 1999, *A&A*, 347, L9
- Woosley, S. E. & Heger, A. 2015, *ApJ*, 810, 34